Thickness-Independent Narrow Resonance in a Stack of Plasmonic Lattices

Ilia M. Fradkin,[1,2,*] Sergey A. Dyakov,[1] and Nikolay A. Gippius[1]

[1] *Skolkovo Institute of Science and Technology, Nobel Street 3, Moscow 143025, Russia*

[2] *Moscow Institute of Physics and Technology, Institutskiy pereulok 9, Moscow Region 141701, Russia*

(Received 14 July 2020; revised 7 September 2020; accepted 10 September 2020; published 13 November 2020)

Plasmonic lattices consisting of nanoparticles in a homogeneous environment are well known for their support of so-called surface lattice resonances. They are associated with localized surface plasmons coupled to each other via photons propagating freely along the structure. Interestingly, such structures provide narrow resonances in plasmonic structures without their coupling to any external high-Q resonators. In this paper, we explore modes in a stack of two identical plasmonic lattices. We demonstrate that such a structure is able to support a mode that is positioned strictly on a Rayleigh anomaly and does not shift with the variation of distance between two lattices over wide limits. Given the fact that the period is the most stably reproduced quantity in an experiment, such behavior can be used to simplify the fabrication of structures with resonances at desired energies. The application of this effect can be very useful in lasing, light emission from metasurfaces, optical filters, and many other optical devices.

DOI: 10.1103/PhysRevApplied.14.054030

I. INTRODUCTION

Plasmonic lattices form a large class of optical metasurfaces. In recent years, they have gained great attention due to the combination of a design that makes qualitative analysis simple and unique optical properties. Hybrid photonic structures with inclusions of such lattices confine light and enhance light-matter interaction due to plasmonic resonances, whereas the photonic counterpart provides high-quality resonances. These prerequisites lead to an application of such structures for sensing [1–4], light-emission enhancement and routing [5–9], lasing [10–14], holography [15–17], and many other purposes.

Plasmonic lattices in homogeneous environments are well known for specific nontypical surface lattice resonances (SLRs), also known as lattice plasmon resonances. The SLRs are the modes associated with collective oscillations of individual nanoparticles coupled to each other by free photons propagating along the lattice. These resonances are unique since they potentially allow us to achieve very narrow lines in a plasmonic structure without the implementation of a photonic waveguide or any other high-Q dielectric resonator. Such resonances have been thoroughly investigated both theoretically and experimentally [2,6,7,11,18–26] and powerful computational methods that can simplify their consideration have been developed [27–29]. However, in most studies, only simple lattices have been considered [2,6,7,11,18,20,22–26,30]. Recently, lattices with several particles in a cell have attracted attention and have been considered in a few studies [31–36]. Nevertheless, there are still many promising designs of plasmonic lattices, particularly in homogeneous media, that are of great interest but have not yet been considered.

In this paper, we consider a stack of two plasmonic lattices in a homogeneous environment. We study the symmetries of their modes, observe Fabry-Perot resonances, show and explain the coupling of the surface lattice resonances, and demonstrate that in some cases one of the hybridized SLRs arises exactly on the Rayleigh anomaly (RA) [37]. Such a mode is narrower than a typical lattice resonance and is observed over a wide range of distances between lattices. Our results show that this effect can be used efficiently to set the resonance energy precisely, since it is determined only by the structure period, which is the quantity that is most stably reproduced in an experiment. Although we do not provide a comprehensive classification of two-lattice structures and their modes, the presented techniques can be further applied to explore any similar structures.

II. RESULTS AND DISCUSSION

The physical phenomena demonstrated in this paper do not require a specific choice of materials and particles, so we consider simple square lattices of silver nanodisks embedded in silica ($\varepsilon_{SiO_2} = 2.1$). The nanodisks have a radius of 30 nm, a height of 20 nm, and are described by Johnson and Christy optical constants [38]. The period of

*Ilia.Fradkin@skoltech.ru

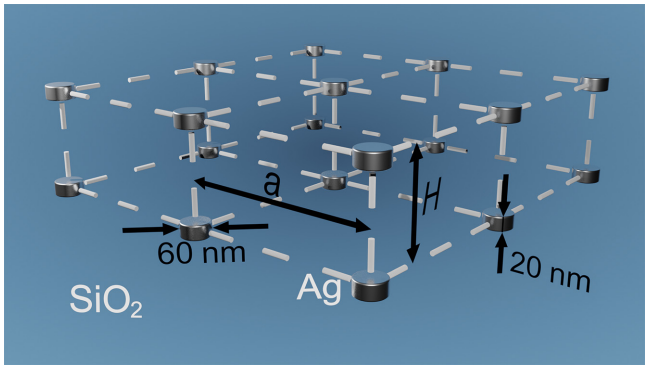

FIG. 1. A schematic of the stack of two plasmonic lattices. Each lattice is square and consists of silver nanodisks. The whole structure is embedded into an infinite layer of silica.

the structure, a, and the thickness, H (see Fig. 1), are varied throughout the study.

Small plasmonic nanoparticles can be effectively described in the dipole approximation if their dimensions are much smaller than both the distance between them and the wavelength of light. Such an approach has been developed and applied for plasmonic lattices in many papers [5,6,10,19,20,22,24,27,30,33,34,39–41] and has proved itself to be much faster than widespread finite-element method (FEM) or finite-difference time-domain (FDTD) approaches. Also, additional accounting for magnetic dipoles can allow us to consider bianisotropic (nonlocal) effects [36,42] and observe the excitation of bound states in the continuum (BICs), also known as trapped modes [43]. Concurrently, the high precision of the dipole approximation allows us to trust the results and use them for analysis of physical effects as well as for the design of optical devices. In this paper, all the calculations are conducted via the method developed by our group in recent papers [32,44,45], which allows us to construct a scattering matrix of a plasmonic lattice in the dipole approximation [46] and integrate it using the Fourier modal method (FMM) [47], also known as rigorous coupled-wave analysis (RCWA) [48]. In such a representation, the interaction of any number of vertically spaced lattices is easily accounted for by the calculation of their combined scattering matrix [49]. Here, we consider only infinite lattices that are suitable for our computational approach but finite-size effects can potentially be studied [6,50,51] and are also of great interest.

At the same time, in order to provide an intuitive explanation of the demonstrated effects and an interpretation of the results, here we apply the dipole model, which accounts for two spaced lattices as constituents of a single layer. The dipole moments of particles, $\mathbf{P}$, in a certain cell can be found by an application of the polarizability tensor, $\hat{\alpha}$, to a background electric field acting on them:

$$\begin{pmatrix}\mathbf{P}_1\\ \mathbf{P}_2\end{pmatrix} = \begin{pmatrix}\hat{\alpha} & 0\\ 0 & \hat{\alpha}\end{pmatrix}\begin{pmatrix}\mathbf{E}_1^{\mathrm{bg}}\\ \mathbf{E}_2^{\mathrm{bg}}\end{pmatrix}, \tag{1}$$

where the indices $1,2$ correspond to either the upper or the lower lattice. The dipole moments of particles in different cells are trivially connected with each other by Bloch's theorem. Taking into account that the background field is the sum of an external electric field, $\mathbf{E}^0$, of illuminating light and the field rescattered by neighboring particles of both lattices, we obtain the self-consistent system of equations:

$$\begin{pmatrix}\mathbf{P}_1\\ \mathbf{P}_2\end{pmatrix} = \begin{pmatrix}\hat{\alpha} & 0\\ 0 & \hat{\alpha}\end{pmatrix}\left[\begin{pmatrix}\mathbf{E}_1^0\\ \mathbf{E}_2^0\end{pmatrix} + \begin{pmatrix}\hat{C}_{11} & \hat{C}_{12}\\ \hat{C}_{21} & \hat{C}_{22}\end{pmatrix}\begin{pmatrix}\mathbf{P}_1\\ \mathbf{P}_2\end{pmatrix}\right], \tag{2}$$

where the $\hat{C}$ blocks are lattice sums of dyadic Green's functions [27,36], also known as dynamic interaction constants [52]. The diagonal blocks are associated with the self-action of lattices and since the background environment is homogeneous, they are equal in our case: $\hat{C}_{11} = \hat{C}_{22}$. The off-diagonal blocks correspond to an interaction of the upper and lower lattices. It should be especially noted that the off-diagonal blocks are not equal to each other in the general case, $\hat{C}_{12} \neq \hat{C}_{21}$, which is discussed in the Supplemental Material [53].

Due to the absence of a relative in-plane shift of two lattices and the subsequent high symmetry of the considered structure (see Fig. 1), the off-diagonal elements of all the $\hat{C}$ blocks vanish for normally incident light ($\mathbf{k}_\parallel = 0$). Moreover, the off-diagonal blocks become equal to each other in this case (see the Supplemental Material [53]). This means that the x-, y-, and z-polarized solutions get separated in terms of both dipole moments and incident light. Hence, the z component of the dipole moment cannot be excited by normally incident light. Concurrently, the x- and y-polarized solutions are equivalent to each other, which allows us to consider only x polarization without loss of generality:

$$\begin{pmatrix}P_1^x\\ P_2^x\end{pmatrix} = \begin{pmatrix}\alpha_{xx} & 0\\ 0 & \alpha_{xx}\end{pmatrix} \times\left[\begin{pmatrix}E_1^{0x}\\ E_2^{0x}\end{pmatrix} + \begin{pmatrix}C_{11}^{xx} & C_{12}^{xx}\\ C_{21}^{xx} & C_{11}^{xx}\end{pmatrix}\begin{pmatrix}P_1^x\\ P_2^x\end{pmatrix}\right]. \tag{3}$$

The fact that $C_{12}^{xx} = C_{21}^{xx}$ (see the Supplemental Material [53]) makes the equations symmetric. In turn, such a symmetric system supports two modes corresponding to in-phase and antiphase dipole-moment oscillations, which we denote by subscripts A and B. Further, we refer to modes A

and B as even and odd, respectively. An appropriate choice of the basis makes the system diagonal:

$$\begin{pmatrix} P_A \\ P_B \end{pmatrix} = \frac{\alpha_{xx}}{\sqrt{2}} \begin{pmatrix} E_1^{0x} + E_2^{0x} \\ E_1^{0x} - E_2^{0x} \end{pmatrix} + \alpha_{xx} \begin{pmatrix} C_{11}^{xx} + C_{12}^{xx} & 0 \\ 0 & C_{11}^{xx} - C_{12}^{xx} \end{pmatrix} \begin{pmatrix} P_A \\ P_B \end{pmatrix}, \quad (4)$$

where

$$\begin{pmatrix} P_A \\ P_B \end{pmatrix} = \frac{1}{\sqrt{2}} \begin{pmatrix} 1 & 1 \\ 1 & -1 \end{pmatrix} \begin{pmatrix} P_1^x \\ P_2^x \end{pmatrix}. \quad (5)$$

The solution of this system gives us amplitudes of the modes in the explicit form

$$P_A = \frac{E_1^{0x}(1 + e^{ikH})/\sqrt{2}}{\alpha_{xx}^{-1} - (C_{11}^{xx} + C_{12}^{xx})}, \quad (6)$$

$$P_B = \frac{E_1^{0x}(1 - e^{ikH})/\sqrt{2}}{\alpha_{xx}^{-1} - (C_{11}^{xx} - C_{12}^{xx})}, \quad (7)$$

where $k = k_0\sqrt{\varepsilon_{SiO_2}}$ is the wave number in silica and the external incident light is assumed to come from above. It is important to emphasize that these expressions are strict in the framework of the dipole approximation. However, we derive them not in order to conduct computations and obtain the precise solution, but for qualitative analysis.

As a first example, we consider the structure of period $a = 395$ nm and compute its spectra as a function of its thickness, H. Since ordinary lattice plasmons are observed in the close vicinity of Rayleigh anomalies (RAs), we consider energies near the first-order RAs: $\langle \pm 1, 0 \rangle$, and $\langle 0, \pm 1 \rangle$. By means of our approach [32,44,45], we calculate $|P_A|$ and $|P_B|$ as they are most convenient for analysis [Figs. 2(a) and 2(b)]. There are lots of modes and peculiarities in these figures that we explain stepwise below.

In the expressions for the mode amplitudes [see Eqs. (6) and (7)], the numerators represent the effectiveness of incident light coupling to corresponding modes. They are periodic functions of H, which oscillate between their maxima and zero. From the explicit expressions [Eqs. (6) and (7)], we derive that the amplitude of even mode A is zero for $kH = \pi + 2\pi n$ and the amplitude of odd mode B for $kH = 2\pi n$, $n \in \mathbb{N}$. In other words, when these conditions are satisfied, normally incident light is unable to excite one mode or another because of the symmetry mismatch. As we can see from Figs. 2(a) and 2(b), the heavy green dashed lines that correspond to these conditions indeed lie in a dark-blue zone of no excitation. The light green lines are defined by the same formulas but correspond to the excitation maxima of complementary modes. When the photon energy matches the level of the RA, its wavelength in silica is equal to the period of the structure ($k = 2\pi/a$) by definition, which means that the intersection of the heavy green lines with the white dotted line of the RA occurs at $H = a/2 + an$ or $H = an$, depending on the symmetry.

As the next step, we consider the hybridization of lattice plasmons. Taking into account the modes' parity and their proximity to RAs, one can easily obtain that the even lattice mode A (or odd lattice mode B) cannot be excited at $H \approx 200$, 600, and 1000 nm (or $H \approx 0$, 400, and 800 nm). However, these modes can be observed at thicknesses in between these values, as is confirmed by Figs. 2(a) and 2(b). In Ref. [31], it has been shown that in the case when

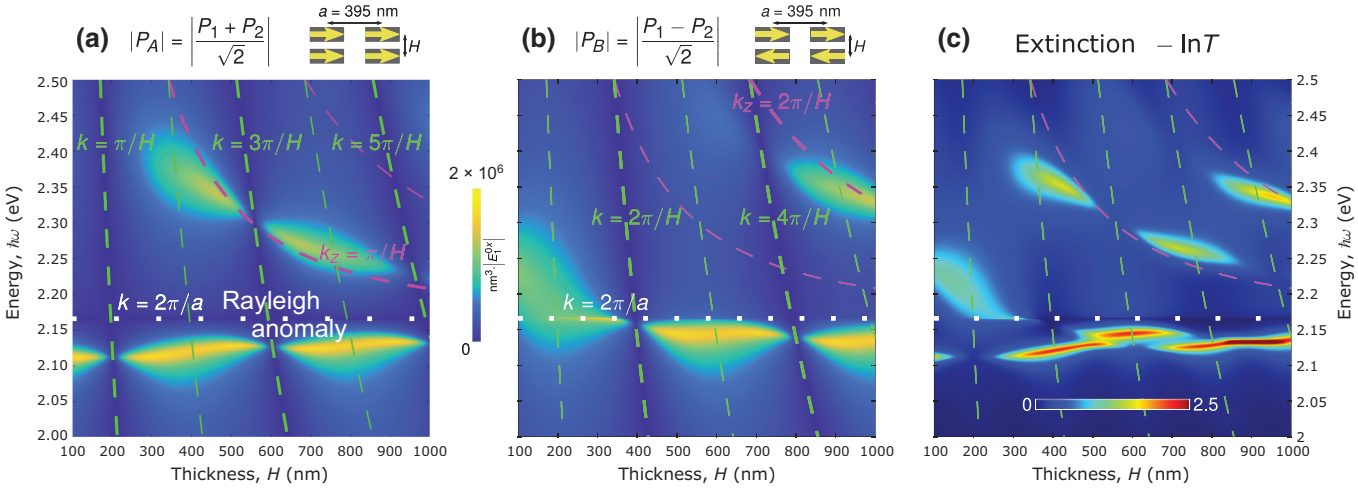

FIG. 2. The thickness-dependent spectra of the (a) even- and (b) odd-mode amplitudes. The white dotted lines correspond to the energy of the RA and the heavy (or light) green dashed lines indicate the condition of no excitation (or maximum excitation) in (a) and (b). The magenta lines show the estimations of the position of the Fabry-Perot modes. In (a) and (b), the heavy lines correspond to modes of the even and odd parities, respectively. (c) The extinction spectrum of the same structure for normal light incidence.

both lattices lie in the same plane ($H = 0$) and the relative in-plane shift between them tends to zero, the x components of the diagonal and off-diagonal blocks C^{xx} are equal $C^{xx}_{11} = C^{xx}_{12}$ in the close vicinity of the first RA. However, since both of them diverge at the RA and this divergence is due to harmonics propagating along the structure ($k_z \approx 0$), this relation remains valid for $H > 0$ in some limits. Therefore, the lattice sums add up in the denominator for the mode-A amplitude [Eq. (6)] and we observe the lattice plasmon in Fig. 2(a) when the condition $\mathrm{Re}\,\alpha^{-1}_{xx} = 2C^{xx}_{11}$ is satisfied. Also, in this case, the sums diverge on the RA and P_A goes to zero, exactly as in the case of a single lattice.

However, a much more interesting situation is observed for the odd mode B, where the lattice sums cancel each other out, which means that in order to obtain meaningful results, we should accurately account for their finite difference and for the finite contributions of other harmonics. Here, we analyze analytical expressions to explain the most important effects.

It is convenient to represent the lattice sums in the vicinity of the RA as a sum of a diverging term (originating from diffraction harmonics of the first order) and the remaining part: $C^{xx}_{11} = (4\pi/s)(ik_0^2/k_z) + \tilde{C}^{xx}_{11}$ and $C^{xx}_{12} = (4\pi/s)(ik_0^2/k_z)\,e^{ik_zH} + \tilde{C}^{xx}_{12}(H)$, where $k_z = \sqrt{k^2 - (2\pi/a)^2}$ (see the Supplemental Material [53]). Importantly, $\tilde{C}^{xx}_{11}$ is a smooth function of the energy near the RA and does not depend on H at all, whereas $\tilde{C}^{xx}_{12}$ is also smooth but depends on H. For relatively large thicknesses (greater than 150–200 nm), this dependence is mostly determined by the zero-order channel, which forces it to oscillate with a period of the wavelength in silica, which is close to the period of the structure, a, near the RA. In this way, the denominator can be represented as follows:

$$\alpha^{-1}_{xx} - C^{xx}_{11} + C^{xx}_{12} = \alpha^{-1}_{xx} + \frac{4\pi}{s}\frac{ik_0^2}{k_z}(e^{ik_zH} - 1) - \tilde{C}^{xx}_{11} + \tilde{C}^{xx}_{12}(H). \quad (8)$$

The main intrigue comes from the expression $(e^{ik_zH} - 1)/k_z$, which is not determined at the energy of RA, but is easily resolved by a Taylor-series expansion:

$$\begin{aligned}\alpha^{-1}_{xx} - C^{xx}_{11} + C^{xx}_{12} &\approx \alpha^{-1}_{xx} + \frac{4\pi}{s}\frac{ik_0^2}{k_z}(ik_zH - k_z^2H^2/2) - \tilde{C}^{xx}_{11} + \tilde{C}^{xx}_{12}(H)\\ &= \alpha^{-1}_{xx} - \frac{4\pi k_0^2}{s}H - \frac{4\pi k_0^2}{s}ik_zH^2/2 - \tilde{C}^{xx}_{11} + \tilde{C}^{xx}_{12}(H).\end{aligned} \quad (9)$$

We see that divergent contributions compensate each other effectively for small thicknesses H. The impact of the remaining smooth term $-\tilde{C}^{xx}_{11} + \tilde{C}^{xx}_{12}(H)$ is not enough to change the behavior of the structure and, therefore, we observe an ordinary wide line of localized plasmon resonance for H less than 200–250 nm [see Fig. 2(b)]. For slightly greater thicknesses, the linear term $(4\pi k_0^2/s)H$ grows in such a way that at some moment it cancels out α^{-1}_{xx} in the denominator of Eq. (7) and from $H \approx 200$ nm we observe the bright yellow line of an odd lattice plasmon right on the RA. The quadratic term in thickness $-(4\pi k_0^2/s)ik_zH^2/2$ does not make any contribution when we consider the energy of the RA ($k_z = 0$); however, it does indicate that there should be a discontinuity of the energy derivative at this point. Moreover, the jump of the derivative grows rapidly with thickness H. As will be shown further [see Figs. 4(b)–4(e)], this leads to strongly non-Lorentzian shapes of resonances. The common effect of the shape violation near the RA has already been considered for some other structures [54]. Interestingly, this resonance is much narrower than conventional lattice plasmons (see the Supplemental Material [53]). With the further increase of H, the resonance condition on the RA remains valid until approximately 350 nm, which is very close to the heavy green line of no excitation. When this resonance comes back after the intersection with this line, it is shifted to the red zone, as it should be in the regime of relatively weak coupling between two lattices. In the limit of a very large thickness, H, there is no difference in energy of the even, odd, and ordinary SLRs of a single lattice.

It is worth noting that although taking into account only first-order harmonics is enough to describe the SLRs in the dipole approximation, they do not provide an insight into the distribution of the near field. Indeed, the high-gradient field of strongly localized surface plasmons dominates the close vicinity of the particles and determines the field enhancement by the lattice resonances. Nevertheless, as long as the dipole approximation is valid, the near field of the particles can be well described by the field used for the calculation of the polarizability tensor multiplied by the corresponding amplitude (see the Supplemental Material [53]).

The last type of resonance to be discussed is a Fabry-Perot-like one. Indeed, we observe several relatively narrow lines above the RA [see Figs. 2(a) and 2(b)]. These modes couple two lattices by Fourier harmonics that have $\mathrm{Re}k_zH \neq 0$ in contrast with SLRs, which are mainly associated with the harmonics that have $\mathrm{Re}\,k_zH = 0$. In order to understand the nature of Fabry-Perot-like modes, we again analyze the denominators from Eqs. (6)–(7), but in a slightly different way. It is obvious that symmetric and antisymmetric resonances arise when $\alpha^{-1}_{xx} - C^{xx}_{11} \approx \pm C^{xx}_{12}(H)$. We again assume that interaction between lattices is mostly determined by the first diffraction harmonics $C^{xx}_{12} \propto (i/k_z)\,e^{ik_zH}$ and, therefore, $k_zH = -\pi/2 \pm \arg(\alpha^{-1}_{xx} - C^{xx}_{11}) + 2\pi n$. An expression $\alpha^{-1}_{xx} - C^{xx}_{11}$

corresponds to a self-action of a lattice. If we consider the spectrum of the single lattice (see the Supplemental Material [53]) then we will see that there is a peak of localized plasmon resonance in the energy range of 2.25–2.35 eV, which means that the phase of the considered expression is approximately $-\pi/2$ in this range. Since $k_x = 2\pi/a$, the even modes, which are associated with $k_z H \approx \pi + 2\pi n$, have the H dependence $k = \sqrt{(2\pi/a)^2 + (\pi + 2\pi n/H)^2}$. For odd modes, we have $k_z H \approx 2\pi n$ and $k = \sqrt{(2\pi/a)^2 + (2\pi n/H)^2}$, respectively. Although these estimations are rough, they are verified by the fact that the corresponding heavy magenta lines match with rigorously calculated resonances [see Figs. 2(a) and 2(b)]. Also it is worth noting that it is better to associate the first branches of this kind with waveguide modes rather than Fabry-Perot ones due to the small phase difference.

The amplitudes of the even and odd modes are very convenient for analysis; however, in practice, we can observe only integral characteristics that provide us with a compound of modes of all parities. For instance, the thickness-dependent extinction spectrum (defined as $-\ln T$, where T is the transmission in the main channel) of normally incident light [Fig. 2(c)] shows that lattice plasmons of complementary symmetries, as well as Fabry-Perot modes, alternate with each other as the thickness increases.

We explain the origin of the resonances in this structure but, for further analysis, it is convenient to find the energies of the resonances as functions of the structure parameters. Conventionally, this is done by searching the poles of some response function (it would be the scattering matrix in our case) in the plane of the complex energy. However, the most exciting odd (B-type) SLR that attracts our attention has a non-Lorentzian shape when located near the RA and, therefore, cannot be described by a single pole. In this work, we do not go into detail about the correct representation of such resonances [54,55] but we find the eigenenergies just as local maxima of the $|P_A(E)|$ and $|P_B(E)|$ functions.

This approach allows us to easily plot the dependence of both SLR energies on the thickness for the same structure. From Fig. 3, we see how the localized surface plasmon resonance (LSPR) gradually transforms into an odd lattice plasmon with the increase in thickness. Moreover, we see that the peak of $|P_B|$ stands on the RA not only for H between approximately 200 and 350 nm but also for smaller thicknesses. Indeed, there is also a small peak, which is not seen by eye, but that does exist. The blue and red lines of lattice plasmons of complementary parities indeed get closer with the increase in thickness and have the same energy for $H \approx 900$ nm. Also, we clearly see the periodic oscillations of each resonance energy, which are due to the already discussed periodic behavior of $\tilde{C}_{12}^{xx}(H)$.

The presented calculations help us to understand the H dependence of all the modes, including the odd B-type

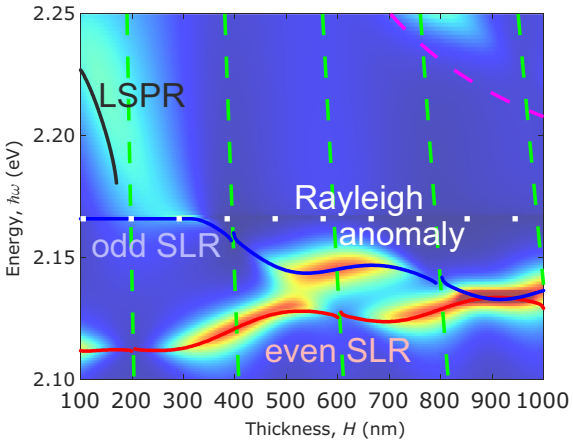

FIG. 3. The thickness dependence of the plasmonic mode energy of the 395-nm-period lattice. The extinction spectrum is shown in slightly faded colors in the background.

SLR. However, it is also important to explore how this mode behaves with variation of the period. In order to do that, we scan for periods and thicknesses simultaneously and plot the extinction of corresponding structures on the RA [see Fig. 4(a)]. First, we see that there is a bright ridge, which corresponds to the resonant conditions of odd SLRs. This ridge is cut by the heavy green dashed lines $H = a, 2a$, which indicate the impossibility of exciting odd modes, as in Fig. 2(b). The cross-hatched region with a white edge in the upper-left part of the graph highlights the area of parameters for which the peak of $|P_B(E)|$ is right on the RA. Interestingly, the edge of this region acts as a crest of the ridge and separates the parameter space into two parts in such a way that half of the bright area corresponds to the resonance peak on the RA and the other half to the peak in its close vicinity.

The shape of the bright ridge line can be easily estimated analytically. Indeed, since we consider the energy of the RA ($E_{\mathrm{RA}} = hc/a\sqrt{\varepsilon_{\mathrm{SiO_2}}}$), then $k_z = 0$ and, according to Eq. (9), the resonant condition, which connects H and a, has the following form:

$$H = \frac{s}{4\pi k_0^2}[\alpha_{xx}^{-1}(E_{\mathrm{RA}}) - \tilde{C}_{11}^{xx}(E_{\mathrm{RA}}, a) + \tilde{C}_{12}^{xx}(E_{\mathrm{RA}}, a, H)]. \quad (10)$$

We have already seen that smooth functions of the energy and period $\tilde{C}$ being added to the inverse polarizability tensor do not have a significant impact on its behavior. Therefore, in order to simplify our estimation, we just omit them but note that $\tilde{C}_{11}^{xx}$ makes a nearly constant complex contribution to the value of H as a function of a, whereas $\tilde{C}_{12}^{xx}$ has a periodic dependence on H that should make the dependence oscillate slightly. Taking into account that

$s = a^2$ and $k_0^2 = 4\pi^2/a^2/\varepsilon_{SiO_2}$ in this case, we obtain

$$H(a) \approx \varepsilon_{SiO_2} \frac{a^4}{16\pi^3} \alpha_{xx}^{-1} \left(\frac{hc}{\sqrt{\varepsilon_{SiO_2}} a} \right). \tag{11}$$

As we see from the red lines in Fig. 4(a), which show both the estimation of the ridge position (the real part) as well as its width (the double imaginary part), indeed match the precise calculation. Moreover, we see that the discrepancy is explained well by an unaccounted-for contribution of secondary terms $\tilde{C}$.

In order to provide a full picture, we compute extinction spectra for several structures, the geometric parameters of which are indicated by markers in Fig. 4(a). The first group, denoted by circles, which are located in the brightest part of the first "hill" of the ridge, is plotted in Fig. 4(b). The main peculiarity of this group is that it illustrates the case in which the RA lies right on the localized resonance and strongly deforms its shape. The green line shows the spectrum of the structure, the parameters of which satisfy the relation $H = a/2$, which means that even modes cannot be excited and, indeed, we observe only a single odd resonance. The blue and red lines that have slightly different thicknesses H both demonstrate small peaks of even lattice modes in the red zone. As we can see from the inset, all the lines have a strongly non-Lorentzian shape and the red line, in contrast to the other ones, has its peak slightly shifted to the red zone, which is in complete agreement with the relative position of the circles with respect to the white line of the ridge.

The next group, depicted by squares, has a period, a, of 395 nm, which corresponds to the structures considered in Figs. 2 and 3. From Fig. 4(c), we see that in this case even SLRs are much more prominent and, besides the two lines of lattice resonances, we observe Fabry-Perot modes in the blue zone as well. Also, the extinction of the red line is strongly suppressed at the RA because of the vicinity of the green line of no excitation.

The diamonds correspond to a period such that odd-mode excitation in the vicinity of the RA is strongly suppressed. From the inset in Fig. 4(d), we see that there is no resonance at all for the green line ($H = a$ in this case). The blue-line peak is so small that it is not seen and the peak of the red one is slightly red shifted, as it should be. Interestingly, the blue line in the vicinity of the RA has a steplike shape, which might be potentially applied, for example, in optical filtering.

The last group of triangles corresponds to the second "hill" of the ridge. We see that in this case, large thicknesses H result in the observation of several Fabry-Perot modes and very narrow lines of lattice modes due to their strong red shift far from the line of the dissipative localized plasmon. Similar to the case considered in Fig. 4(b), the

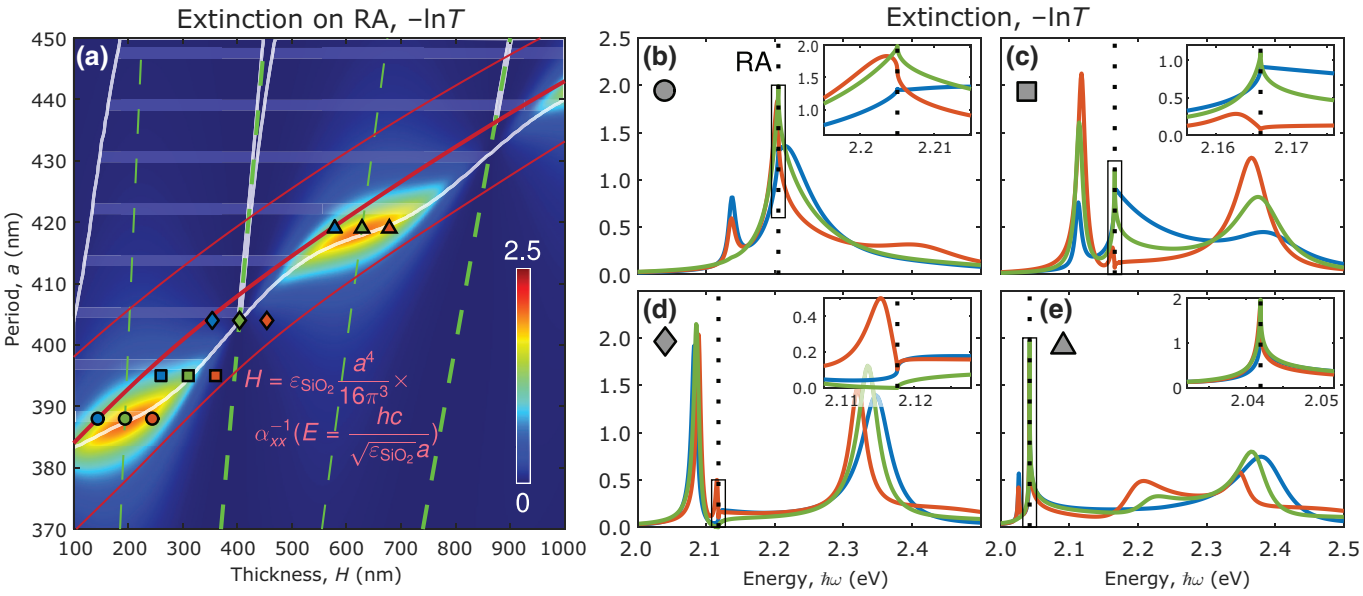

FIG. 4. (a) The extinction of a lattice stack on a RA as a function of its period and thickness. The cross-hatched region with a white edge indicates the area in which the peak of the resonance is located exactly on the RA. The red lines show the naive analytical estimation of the resonance-ridge position and width and the central line corresponds to the real part of the given expression, whereas each of the side lines is shifted in its imaginary part. The multicolored markers correspond to the geometric parameters of the lattices considered in (b)–(e). (b)–(e) The extinction spectra of the structures defined by the markers. The shape of the marker determines the group of the fixed period, whereas the colors in each group correspond to different thicknesses. The insets in each panel show the shapes of lines in close vicinity to the RAs. The enlarged versions of (b)–(e), including a comparison with single-lattice spectra, are presented in the Supplemental Material [53].

green line does not demonstrate the peak of the even-lattice plasmon due to the specific relation between the thickness and the period, $H = 1.5a$. From the inset, we see that there is hardly any significant difference between the lines near the RA. Importantly, these calculations demonstrate that the energy of very narrow resonances can easily be set to E_{RA} by our approach. We hope that this unique property will be useful in problems that require the setting of high-Q resonances at predetermined positions. In the Supplemental Material [53], we provide enlarged plots of the extinction spectra and compare them with the spectra of single plasmonic lattices to show that the odd lattice modes are not only pinned to RAs but are also narrower than ordinary lattice modes.

In this work, we consider the structure of a rather simple design. However, it has lots of degrees of freedom that can be tuned to achieve the desired properties. For example, the relative in-plane shift of two lattices can interchange energies of even and odd modes or mix them. The choice of the shape and size of particles as well as the type of lattice potentially allows us to consider resonances with nontrivial polarization of dipole moments and to demonstrate chiral and spin-orbit effects. Yet another way to go further in the exploration of plasmonic lattices is to increase the number of particles in a cell or the number of layers. Although it is a trivial step in terms of calculation, this can open up exciting opportunities for light manipulation.

III. CONCLUSION

In this paper, we consider a stack of two plasmonic lattices and analyze the hybridized modes emerging in such a structure. We show that aside from localized plasmons, it supports Fabry-Perot modes and lattice plasmons of different symmetries. In particular, the demonstrated antisymmetric SLR is very untypical. It has a very high Q factor for the given detuning from the line of LSPR. Moreover, the very untypical behavior of the lattice sum near the RA, which is due to the strong excitation of almost nonevanescent harmonics, results in pinning of odd SLRs to this RA for a wide range of structure parameters. This makes it possible to set the desired energy precisely by an appropriate period and independently choose its thickness from the wide range of accessible values, which may be used either as an additional tuning parameter for optimization of the desired properties or as a protection against experimental error. Also, it makes stacks of plasmonic lattices attractive for application in problems for which the precise positioning of resonant lines is crucial. In particular, one can employ them in light-emission enhancement and routing, lasing from plasmonic structures, and optical filtering.

ACKNOWLEDGMENTS

The work of I.M.F. was supported by the Foundation for the Advancement of Theoretical Physics and Mathematics "BASIS." The work of S.A.D. and N.A.G. was supported by the Russian Foundation for Basic Research (Grant No. 18-29-20032).

APPENDIX: CALCULATION TECHNIQUES

All the calculations presented in this paper are conducted by the domestically developed hybridized approach [32,44,45], which combines the advantages of the discrete-dipole approximation (DDA) and the scattering-matrix approach of FMM.

At the first stage, we calculate the polarizability tensor of the silver nanodisks (see the Supplemental Material [53]) in COMSOL Multiphysics using FEM [44,45]. The basic principle underlying these calculations is the total and/or scattered field formulation that allows accounting for the action of the background electric field on a certain particle by the primary currents induced inside it.

At the next stage, we calculate the effective polarizability tensor, which accounts for the interaction of the particles in each separate lattice. Such a calculation mostly relies on the lattice sums, which are in turn computed by our domestic approach [44,45]. However, in the case considered, the well-known Ewald summation techniques can potentially be applied.

Finally, we compute the scattering matrix of each layer and the scattering matrix of the whole structure, as their combination [44,45]. Any spectrum (including an extinction one) can be subsequently extracted from the components of the scattering matrix.

The dipole moments of certain particles (considered in the paper) are easily determined in the framework of our approach as intermediate quantities in the described chain of calculations.

[1] Y. Shen, J. Zhou, T. Liu, Y. Tao, R. Jiang, M. Liu, G. Xiao, J. Zhu, Z.-K. Zhou, X. Wang, C. Jin, and J. Wang, Plasmonic gold mushroom arrays with refractive index sensing figures of merit approaching the theoretical limit, Nat. Commun. **4**, 2381 (2013).

[2] S. R. K. Rodriguez, A. Abass, B. Maes, O. T. Janssen, G. Vecchi, and J. G. Rivas, Coupling Bright and Dark Plasmonic Lattice Resonances, Phys. Rev. X **1**, 021019 (2011).

[3] K. Lodewijks, W. Van Roy, G. Borghs, L. Lagae, and P. Van Dorpe, Boosting the figure-of-merit of LSPR-based refractive index sensing by phase-sensitive measurements, Nano Lett. **12**, 1655 (2012).

[4] F. Sterl, N. Strohfeldt, S. Both, E. Herkert, T. Weiss, and H. Giessen, Design principles for sensitivity optimization in plasmonic hydrogen sensors, ACS Sens. **5**, 917 (2020).

[5] A. Vaskin, R. Kolkowski, A. F. Koenderink, and I. Staude, Light-emitting metasurfaces, Nanophotonics **8**, 1151 (2019).

[6] S. Rodriguez, M. Schaafsma, A. Berrier, and J. G. Rivas, Collective resonances in plasmonic crystals: Size matters, Physica B **407**, 4081 (2012).

[7] R. Guo, S. Derom, A. I. Väkeväinen, R. J. A. van Dijk-Moes, P. Liljeroth, D. Vanmaekelbergh, and P. Törmä, Controlling quantum dot emission by plasmonic nanoarrays, Opt. Express **23**, 28206 (2015).

[8] G. Vecchi, V. Giannini, and J. G. Rivas, Shaping the Fluorescent Emission by Lattice Resonances in Plasmonic Crystals of Nanoantennas, Phys. Rev. Lett. **102**, 146807 (2009).

[9] M. Ramezani, G. Lozano, M. A. Verschuuren, and J. Gómez-Rivas, Modified emission of extended light emitting layers by selective coupling to collective lattice resonances, Phys. Rev. B **94**, 125406 (2016).

[10] A. H. Schokker, F. van Riggelen, Y. Hadad, A. Alù, and A. F. Koenderink, Systematic study of the hybrid plasmonic-photonic band structure underlying lasing action of diffractive plasmon particle lattices, Phys. Rev. B **95**, 085409 (2017).

[11] W. Zhou, M. Dridi, J. Y. Suh, C. H. Kim, D. T. Co, M. R. Wasielewski, G. C. Schatz, T. W. Odom, Lasing action in strongly coupled plasmonic nanocavity arrays, Nat. Nanotechnol. **8**, 506 (2013).

[12] D. Wang, A. Yang, W. Wang, Y. Hua, R. D. Schaller, G. C. Schatz, and T. W. Odom, Band-edge engineering for controlled multi-modal nanolasing in plasmonic superlattices, Nat. Nanotechnol. **12**, 889 (2017).

[13] A. H. Schokker and A. F. Koenderink, Lasing in quasi-periodic and aperiodic plasmon lattices, Optica **3**, 686 (2016).

[14] D. Wang, J. Guan, J. Hu, M. R. Bourgeois, and T. W. Odom, Manipulating light-matter interactions in plasmonic nanoparticle lattices, Acc. Chem. Res. **52**, 2997 (2019).

[15] G. Zheng, H. Mühlenbernd, M. Kenney, G. Li, T. Zentgraf, and S. Zhang, Metasurface holograms reaching 80% efficiency, Nat. Nanotechnol. **10**, 308 (2015).

[16] W. Ye, F. Zeuner, X. Li, B. Reineke, S. He, C.-W. Qiu, J. Liu, Y. Wang, S. Zhang, and T. Zentgraf, Spin and wavelength multiplexed nonlinear metasurface holography, Nat. Commun. **7**, 11930 (2016).

[17] Q. Wei, L. Huang, X. Li, J. Liu, and Y. Wang, Broadband multiplane holography based on plasmonic metasurface, Adv. Opt. Mater. **5**, 1700434 (2017).

[18] R. Guo, T. K. Hakala, and P. Törmä, Geometry dependence of surface lattice resonances in plasmonic nanoparticle arrays, Phys. Rev. B **95**, 155423 (2017).

[19] B. Auguié and W. L. Barnes, Collective Resonances in Gold Nanoparticle Arrays, Phys. Rev. Lett. **101**, 143902 (2008).

[20] B. B. Rajeeva, L. Lin, and Y. Zheng, Design and applications of lattice plasmon resonances, Nano Res. **11**, 4423 (2018).

[21] V. Kravets, F. Schedin, and A. Grigorenko, Extremely Narrow Plasmon Resonances Based on Diffraction Coupling of Localized Plasmons in Arrays of Metallic Nanoparticles, Phys. Rev. Lett. **101**, 087403 (2008).

[22] V. Kravets, A. Kabashin, W. Barnes, and A. Grigorenko, Plasmonic surface lattice resonances: A review of properties and applications, Chem. Rev. **118**, 5912 (2018).

[23] W. Wang, M. Ramezani, A. I. Väkeväinen, P. Törmä, J. G. Rivas, and T. W. Odom, The rich photonic world of plasmonic nanoparticle arrays, Mater. Today **21**, 303 (2017).

[24] L. Zhao, K. L. Kelly, and G. C. Schatz, The extinction spectra of silver nanoparticle arrays: Influence of array structure on plasmon resonance wavelength and width, J. Phys. Chem. B **107**, 7343 (2003).

[25] V. Gerasimov, A. Ershov, R. Bikbaev, I. Rasskazov, I. Timofeev, S. Polyutov, and S. Karpov, Engineering mode hybridization in regular arrays of plasmonic nanoparticles embedded in 1D photonic crystal, J. Quantit. Spectrosc. Radiat. Transf. **224**, 303 (2019).

[26] V. I. Zakomirnyi, I. L. Rasskazov, V. S. Gerasimov, A. E. Ershov, S. P. Polyutov, and S. V. Karpov, Refractory titanium nitride two-dimensional structures with extremely narrow surface lattice resonances at telecommunication wavelengths, Appl. Phys. Lett. **111**, 123107 (2017).

[27] Y. Chen, Y. Zhang, and A. F. Koenderink, General point dipole theory for periodic metasurfaces: Magnetoelectric scattering lattices coupled to planar photonic structures, Opt. Express **25**, 21358 (2017).

[28] V. E. Babicheva and A. B. Evlyukhin, Metasurfaces with electric quadrupole and magnetic dipole resonant coupling, ACS Photonics **5**, 2022 (2018).

[29] V. E. Babicheva and A. B. Evlyukhin, Analytical model of resonant electromagnetic dipole-quadrupole coupling in nanoparticle arrays, Phys. Rev. B **99**, 195444 (2019).

[30] F. J. García de Abajo, Colloquium: Light scattering by particle and hole arrays, Rev. Mod. Phys. **79**, 1267 (2007).

[31] S. Baur, S. Sanders, and A. Manjavacas, Hybridization of lattice resonances, ACS Nano **12**, 1618 (2018).

[32] I. M. Fradkin, S. A. Dyakov, and N. A. Gippius, Nanoparticle lattices with bases: Fourier modal method and dipole approximation, Phys. Rev. B **102**, 045432 (2020).

[33] R. Kolkowski and A. F. Koenderink, Lattice resonances in optical metasurfaces with gain and loss, Proc. IEEE, **108**, 795 (2020).

[34] A. D. Humphrey and W. L. Barnes, Plasmonic surface lattice resonances on arrays of different lattice symmetry, Phys. Rev. B **90**, 075404 (2014).

[35] D. Becerril, O. Vázquez, D. Piccotti, E. M. Sandoval, T. Cesca, G. Mattei, C. Noguez, and G. Pirruccio, Diffractive dipolar coupling in non-Bravais plasmonic lattices, Nanoscale Adv. **2**, 1261 (2020).

[36] A. Kwadrin and A. F. Koenderink, Diffractive stacks of metamaterial lattices with a complex unit cell: Self-consistent long-range bianisotropic interactions in experiment and theory, Phys. Rev. B **89**, 045120 (2014).

[37] D. Maystre, in *Plasmonics* (Springer, Berlin, Heidelberg, 2012), pp. 39–83.

[38] P. B. Johnson and R. W. Christy, Optical constants of the noble metals, Phys. Rev. B **6**, 4370 (1972).

[39] O. Reshef, M. Saad-Bin-Alam, M. J. Huttunen, G. Carlow, B. T. Sullivan, J.-M. Ménard, K. Dolgaleva, and R. W. Boyd, Multiresonant high-Q plasmonic metasurfaces, Nano Lett. **19**, 6429 (2019).

[40] A. Berkhout and A. F. Koenderink, Perfect absorption and phase singularities in plasmon antenna array etalons, ACS Photonics **6**, 2917 (2019).

[41] A. B. Evlyukhin, C. Reinhardt, A. Seidel, B. S. Luk'yanchuk, and B. N. Chichkov, Optical response features of Si-nanoparticle arrays, Phys. Rev. B **82**, 045404 (2010).

[42] E. S. Goerlitzer, R. Mohammadi, S. Nechayev, K. Volk, M. Rey, P. Banzer, M. Karg, and N. Vogel, Chiral surface lattice resonances, Adv. Mater. **32**, 2001330 (2020).

[43] A. B. Evlyukhin, V. R. Tuz, V. S. Volkov, and B. N. Chichkov, Bianisotropy for light trapping in all-dielectric metasurfaces, Phys. Rev. B **101**, 205415 (2020).

[44] I. M. Fradkin, S. A. Dyakov, and N. A. Gippius, Fourier modal method for the description of nanoparticle lattices in the dipole approximation, arXiv:1812.11359 [physics.optics].

[45] I. M. Fradkin, S. A. Dyakov, and N. A. Gippius, Fourier modal method for the description of nanoparticle lattices in the dipole approximation, Phys. Rev. B **99**, 075310 (2019).

[46] P. C. Chaumet, A. Rahmani, and G. W. Bryant, Generalization of the coupled dipole method to periodic structures, Phys. Rev. B **67**, 165404 (2003).

[47] S. G. Tikhodeev, A. Yablonskii, E. Muljarov, N. A. Gippius, and T. Ishihara, Quasiguided modes and optical properties of photonic crystal slabs, Phys. Rev. B **66**, 045102 (2002).

[48] M. Moharam, E. B. Grann, D. A. Pommet, and T. Gaylord, Formulation for stable and efficient implementation of the rigorous coupled-wave analysis of binary gratings, JOSA A **12**, 1068 (1995).

[49] D. Y. K. Ko and J. Inkson, Matrix method for tunneling in heterostructures: Resonant tunneling in multilayer systems, Phys. Rev. B **38**, 9945 (1988).

[50] V. Zakomirnyi, A. Ershov, V. Gerasimov, S. Karpov, H. Ågren, and I. Rasskazov, Collective lattice resonances in arrays of dielectric nanoparticles: A matter of size, Opt. Lett. **44**, 5743 (2019).

[51] L. Zundel and A. Manjavacas, Finite-size effects on periodic arrays of nanostructures, J. Phys.: Photonics **1**, 015004 (2018).

[52] P. A. Belov and C. R. Simovski, Homogenization of electromagnetic crystals formed by uniaxial resonant scatterers, Phys. Rev. E **72**, 026615 (2005).

[53] See the Supplemental Material at http://link.aps.org/supplemental/10.1103/PhysRevApplied.14.054030 for (i) the the energy dependence of the polarizability of the silver particles and the spectra of the plasmonic lattice, which constitutes the considered stack; (ii) the consideration of the dyadic Green's function and lattice sums and a brief analysis of the explicit expressions and their symmetries; (iii) a comparison of the spectra of stacks with the spectra of corresponding single lattices and of the spectra obtained in the dipole approximation with ones calculated using COMSOL MULTIPHYSICS; and (iv) a demonstration of the near fields of the resonances.

[54] A. Akimov, N. A. Gippius, and S. G. Tikhodeev, Optical fano resonances in photonic crystal slabs near diffraction threshold anomalies, JETP Lett. **93**, 427 (2011).

[55] T. Weiss, M. Schäferling, H. Giessen, N. Gippius, S. Tikhodeev, W. Langbein, and E. Muljarov, Analytical normalization of resonant states in photonic crystal slabs and periodic arrays of nanoantennas at oblique incidence, Phys. Rev. B **96**, 045129 (2017).